Clinical & Experimental Immunology
The Journal of Translational Immunology

Clinical and Experimental Immunology ORIGINAL ARTICLE doi: 10.1111/cei.13154

S100A8/A9 promotes parenchymal damage and renal fibrosis in obstructive nephropathy

A. Tammaro,* S. Florquin,* M. Brok,* N. Claessen,* L. M. Butter,* G. J. D. Teske,* O. J. de Boer,* T. Vogl,† J. C. Leemans*[1] and M. C. Dessing*[1]

*Department of Pathology, Amsterdam UMC, Univ(ersity) of Amsterdam, Amsterdam, the Netherlands, and †Institute of Immunology, University of Münster, Münster, Germany

Accepted for publication 26 April 2018
Correspondence: A. Tammaro, Department of Pathology, Amsterdam UMC, Univ(ersity) of Amsterdam, Room L2-112, Meibergdreef 09, Amsterdam 1105AZ, the Netherlands.
E-mail: a.tammaro@amc.uva.nl

[1]These authors contributed equally to this study.

Summary

Despite advances in our understanding of the mechanisms underlying the progression of chronic kidney disease and the development of fibrosis, only limited efficacious therapies exist. The calcium binding protein S100A8/A9 is a damage-associated molecular pattern which can activate Toll-like receptor (TLR)-4 or receptor for advanced glycation end-products (RAGE). Activation of these receptors is involved in the progression of renal fibrosis; however, the role of S100A8/A9 herein remains unknown. Therefore, we analysed S100A8/A9 expression in patients and mice with obstructive nephropathy and subjected wild-type and S100A9 knock-out mice lacking the heterodimer S100A8/A9 to unilateral ureteral obstruction (UUO). We found profound S100A8/A9 expression in granulocytes that infiltrated human and murine kidney, together with enhanced renal expression over time, following UUO. S100A9 KO mice were protected from UUO-induced renal fibrosis, independently of leucocyte infiltration and inflammation. Loss of S100A8/A9 protected tubular epithelial cells from UUO-induced apoptosis and critical epithelial–mesenchymal transition steps. *In-vitro* studies revealed S100A8/A9 as a novel mediator of epithelial cell injury through loss of cell polarity, cell cycle arrest and subsequent cell death. In conclusion, we demonstrate that S100A8/A9 mediates renal damage and fibrosis, presumably through loss of tubular epithelial cell contacts and irreversible damage. Suppression of S100A8/A9 could be a therapeutic strategy to halt renal fibrosis in patients with chronic kidney disease.

Keywords: damage-associated molecular patterns, innate immunity, renal fibrosis, S100 proteins, tubular integrity

Introduction

Fibrotic diseases, including progressive renal diseases, lead to loss of function and organ failure. They represent a major socioeconomic burden and account for at least one-third of deaths worldwide [1]. Renal fibrosis is the final common pathway leading to end-stage renal disease (ESRD), a condition for which no effective treatments exist except for life-long dialysis or renal transplantation [2]. The pathophysiological mechanisms driving the loss of renal function involve four cellular protagonists: myofibroblasts, tubular epithelial cells (TECs), immune cells and endothelial cells which, upon (mal)adaptive activation, induce the progression of tubulo-interstitial fibrosis [3]. Although progress has been made in understanding the molecular mechanisms underlying the development of fibrosis, the failure to limit this process is undeniable. Thus, new avenues need to be explored in order to offer a therapeutic potential for preventing renal fibrosis.

Calprotectin, or the S100A8/S100A9 protein complex, belongs to the S100 calcium-binding protein family. This heterodimer protein is expressed and released by activated phagocytes, mainly neutrophils and macrophages, and has been shown to induce cytoskeleton reorganization [4], chemotaxis [5] and cytokine expression [6,7]. Apart from the above-mentioned intracellular functions, S100A8/A9 is also released upon tissue injury, thereby acting as a damage-associated molecular pattern (DAMP), which mediates the activation of the inflammatory response [8,9]. In the context of obstructive nephropathy, damaged cells

release DAMPs such as S100A8/A9 to alert the immune system [10,11]. In response to the insult, S100A8/A9 functions as an endogenous ligand which binds to pattern recognition receptors (PRRs), including Toll-like receptor (TLR)-4 [12,13] and the receptor for advanced glycation end-products (RAGE) [14,15]. Both receptors are expressed by macrophages and TECs following ureteral obstruction [16,17], which can initiate the inflammatory response and are involved in processes related to tissue repair. Also, chronic inflammation may perpetuate tissue injury leading to the development of fibrosis [3]. Indeed, several studies have demonstrated that TLR-4 and RAGE represent key factors of chronic kidney disease (CKD) progression through modulation of interstitial fibrosis [17,18]. As these receptors are crucial for host defence it might be more interesting to target their ligands instead. Thus, we investigated the role of their shared ligand S100A8/A9 in the pathogenesis of renal fibrosis. To assess the contribution of S100A8/A9 in the progression of renal fibrosis we subjected wild-type (WT) and S100A9 knock-out (KO) mice to UUO and determined its expression, location and function.

Materials and methods

Patients

Renal biopsies (n = 3) were obtained from patients diagnosed with obstructive hydronephrosis, characterized by extensive fibrosis and tubular atrophy or healthy renal tissue, at the Academic Medical Center (University of Amsterdam), as described previously [19]. All biopsies were taken for diagnostic purposes only. For the present study, only left-over biological material was used, delinked from patient records, and as such was not subjected to any requirement for ethical review or approval according to Dutch law when patients have made no objection (Article 7:467 BW Book 7). We have only used the material of patients with no objection.

Experimental animals and procedure

The Institutional Animal Care and Use Committee of the University of Amsterdam approved all experiments for the animal study, in compliance with the Animal Research: Reporting of In Vivo Experiments (ARRIVE) guidelines (NC3Rs). The study was designed with two experimental groups: (1) C57Bl/6 WT controls (n = 8) and (2) S100A9 KO animals (n = 8) and four time-points (from days 1, 3, 7 and 14 of sacrifice) for each experimental group. Each experimental group was divided into two cages of three and five animals. The total number of mice for the experimental group was 32. Genetic deletion of S100A8 leads to embryonic lethality [20]. We therefore used S100A9-deficient mice that lack functional calprotectin complex and display almost undetectable levels of S100A8 protein. These mice were generated as described previously [21] and back-crossed to a C57Bl/6 genetic background. Animals were bred in the animal facility of the Academic Medical Center (AMC) in Amsterdam, the Netherlands. Eight to 10-week-old male mice were used in the experiments. Age- and sex-matched WT C57Bl/6 mice were purchased from Charles River Laboratories (Cologne, Germany). Mice weighed approximately 25 g/mouse. Animals were kept in standard environmental conditions (temperature, humidity, ventilation, light/dark cycle), housed in specific pathogen-free conditions (SPF) with *ad libitum* access to water and food, and allowed to acclimatize for a week before starting the experiment. WT C57Bl/6 and S100A9 KO mice were subjected to progressive renal injury by UUO, as described previously [19]. Briefly, the right ureter was ligated (near the ureteropelvic junction) with suture (6.0 Tyco healthcare) under 2·5% isoflurane-induced anaesthesia and oxygen (via inhalation) through an abdominal incision. The surgical procedure was carried out in the morning under the laminar flow cabinet with a temperature-controlled heating pad. Upon completing surgery, muscle and skin layers were closed with surgical sutures (6.0, Tyco healthcare). Fifty μg/kg buprenorphine was administered through a subcutaneous injection for analgesic purposes (Temgesic, Schering-Plough, Kenilworth, NJ, USA). Animals were sacrificed via cardiac exsanguination followed by cervical dislocation at days 1, 3, 7 and 14 post-surgery. Sham mice were sacrificed at day 1 post-UUO. Contralateral/unobstructed left kidneys were also used as controls.

RNA isolation and reverse transcriptase–polymerase chain reaction (RT–PCR)

Total RNA was isolated from snap-frozen renal tissue using Trizol reagent (Invitrogen, Waltham, MA, USA), according to the manufacturer's protocol. RNA was converted into cDNA by the use of oligo-dT as a primer. Gene expression was analysed by reverse transcriptase-polymerase chain reaction (RT–PCR) with SYBR green PCR master mix on a Lightcycler 480 (Hoffmann-Roche, Basel, Switzerland). Relative expression was analysed using LinRegPCR (developed by Hearth Failure Research Center, University of Amsterdam, the Netherlands). Gene expression was normalized to mouse TATA box-binding protein (*Tbp*) housekeeping gene, n = 7/8 animals per group; see Supporting information, Table S1 for primer sequences.

Plasma biochemical analysis

Plasma levels of creatinine were measured by standard autoanalyser methods at our hospital research services.

Enzyme-linked immunosorbent assay (ELISA) and immunoblot

In order to measure renal S100A8/A9 and transforming growth factor (TGF)-β1 protein, snap-frozen kidney (n = 7/8) tissues were homogenized in Greenberger lysis buffer (150 mM NaCl, 15 mM Tris, 1 mM $MgCl_2$ pH 7.4, 1 mM $CaCl_2$, 1% Triton X-100 and 1% protease inhibitor cocktail (Sigma-Aldrich, Zwijndrecht, the Netherlands). The S100A8/A9 Heterodimer DuoSet and TGF-β1 ELISA kit (R&D Systems, Minneapolis, MN, USA) were used according to the manufacturer's protocol.

Snap-frozen kidneys or cell lysates were used for immunoblotting (n = 2/4). Protein lysates were obtained from snap-frozen kidney tissue or primary TECs derived from *in-vitro* assays. Tissue and cells were lysed in radioimmunoprecipitation assay (RIPA) buffer [50 mM Tris pH 7.5, 0·15 M NaCl, 2 mM ethylenediamine tetraacetic acid (EDTA), 1% deoxycholic acid, 1% NP-40, 4 mM sodium orthovanadate, 10 mM sodium fluoride], supplemented with 1% of protease inhibitor cocktail (Sigma-Aldrich, Zwijndrecht, the Netherlands). Lysates were loaded on a 4–12% Nupage gel and blotted onto a polyvinylidene difluoride (PVDF) membrane. After blocking aspecific signals, blots were incubated overnight at 4°C with different antibodies, as listed in Supporting information, Table S2. Blots were incubated with horseradish peroxidase-conjugated secondary antibodies and detected with enhanced chemiluminescence (ECL) (Pierce, Waltham, MA, USA).

Immunostaining

Renal tissues were fixed in 10% formalin for 24 h, processed and paraffin-embedded. For immunohistochemical staining, 4-μm-thick sections of murine renal tissues (n = 7/8) or human biopsies (n = 3) were treated for 30 min with 0·25% pepsin in 0·1 M HCl at 37°C (for Ly6G) or boiled for 10 min in 10 mM citrate (pH 6.0) (other antibodies), incubated overnight with different primary antibodies, as described in Supporting information, Table S2, and developed using diaminobenzidine (DAB) (Sigma). For collagen staining, slides were incubated with 0·2% Picro Sirius Red (PSR) solution (pH 2.0) for 1 h followed by incubation within 0·01 M HCl. Periodic acid–Schiff diastase (PAS-D) was used to quantify the number of intact tubules, based on morphology, dimensions and brush border presence, as described previously [2]. To quantify the number of apoptotic and proliferating TECs only tubules (not interstitial cells) surrounding glomeruli were included in the count, as shown by the white drawings in the picture. The number of intact tubules and those positive for cleaved caspase-3 or Ki67 were counted within 10 non-overlapping high-power fields (HPF) (×40 magnification) in a blinded manner. The amount of positive staining for F4/80, alpha smooth muscle actin (αSMA), collagen I, PSR, intercellular adhesion molecule 1 (ICAM-1), S100A8 and S100A9 was quantified with ImageJ software, Fiji (National Institutes of Health, Bethesda, MD, USA), a computer-based imaging analysis for reliable biomarker quantitation which is applied widely for tissue-based research.

For sequential immunohistochemistry, sections were labelled and stained with NovaRed, as described previously [22]. After each staining slides were acquired on a digital slide scanner (IntelliSite Pathology Ultra Fast Scanner; Philips, Eindhoven, the Netherlands). Afterwards, coverslips were removed and the sections were stripped by incubation for 30 min in 1 M Tris–HCl (pH 7.5) supplemented with 2% (v/v) sodium dodecyl sulphate and 0·7% (v/v) β-mercaptoethanol at 50°C, followed by rinsing with tap water. Complete removal of the stain was ensured by visual inspection. Three sequential stainings (mouse: S100A8, S100A9 and Ly6G/F480; human: S100A8/S100A9, CD15 and CD68) were performed on the same section. Overlay images were obtained as described previously by our group [22].

For immunofluorescence staining, paraffin-embedded tissues from T14 post-UUO were incubated with biotin–dolichos biflorus agglutinin (DBA: collecting duct marker) and lotus tetragonolobus lectin (LTL: proximal tubule marker) followed by streptavidin fluorescein isothiocyanate (FITC). Primary antibodies incubation followed the lectin staining. Rat-anti-S100A8 and S100A9 primary antibodies were detected by rabbit anti-rat Texas Red. Nuclei were stained with Hoechst. Pictures were taken with a fluorescence light microscope (Leica, Wetzlar, Germany; magnification ×40).

Reagents were used according to the manufacturer's protocol.

In-vitro assays

For *in-vitro* assays, primary, immortalized proximal TECs (IM-PTEC) and polarized TECs [Madin–Darby canine kidney cells (MDCK)] were used. Primary TECs were isolated from kidneys of C57Bl/6 WT mice (n = 4), as described previously [23]. IM-PTECs were cultured in hexokinase 2 (HK2) medium supplemented with interferon gamma at 33°C. A week before the experiment, IM-PTEC cells were transferred to a 37°C incubator in order to lose SV40 expression [24]. MDCK cells were cultured on collagen-coated coverslips in HK2 medium. Cells were stimulated with different concentrations of recombinant S100A8/A9 (rS100A8/A9) (kindly provided by T. Vogl) and/or recombinant TGF-β1 (rTGF-β1) (Pepscan, Lelystad, the Netherlands), as described in the figure legends, for 24 h.

Cell death assays were performed as follows. Cells were detached with trypsin, washed once with phosphate-buffered saline (PBS) followed by washing with annexin V buffer [500 ml: 1·19 g HEPES, 4·4 g NaCl, 0·19 g KCl, 0·1 g $CaCl_2$, 0·1 g $MgCl_2$, 1 ml/ml glucose and 0·5% bovine serum albumin (BSA), pH 7.3]. Subsequently, cells were incubated with annexin V for 20 min on ice in the dark. Propidium iodide (PI) or To-Pro3 (Thermo Fisher,

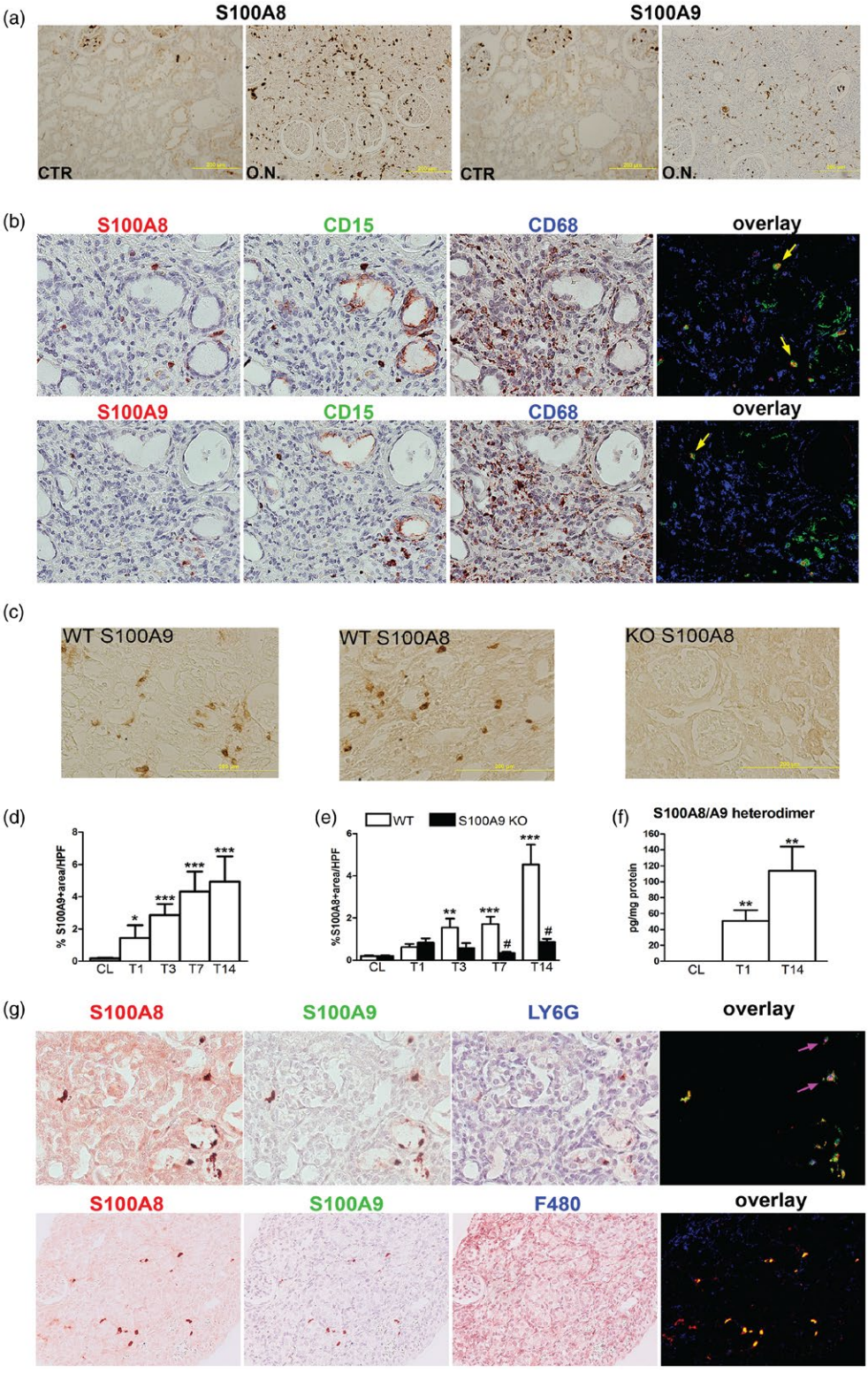

Fig. 1. Human and murine S100A8/A9 expression during obstructive nephropathy. (a) Immunohistochemistry for human S100A8 and S100A9 on healthy tissue (CTR) and from kidney biopsies of patients with obstructive hydronephrosis (ON). (b) Representative examples of original immunostaining and composite overlays for S100A8 or S100A9 (red), CD15 (green) and CD68 (blue) on obstructive nephropathy biopsies. Composite images, obtained with Image J, reveal only the triple overlay between S100A8/S100A9 and CD15 (yellow cells and arrow) (magnification ×40). (c) Representative pictures of murine S100A8/A9 staining in kidney sections from wild-type (WT) and S100A9 knock-out (KO) mice. (d) Quantification of S100A9 in contralateral kidneys (CL) (grey bar) and WT mice (white bars) upon 1, 3, 7 and 14 days of unilateral ureteral obstruction (UUO). (e) Quantification of S100A8 in CL kidneys and upon 1, 3, 7 and 14 days of UUO in sham WT and S100A9 KO mice. (f) Murine S100A8/A9 protein complex levels in CL kidneys or following 1 and 14 days of UUO in WT mice as measured by enzyme-linked immunosorbent assay (ELISA). Protein expression was corrected for total protein levels in renal tissue. (g) Representative examples of original immunostaining and composite overlays for S100A8 (red), S100A9 (green) and Ly-6G or F480 (blue) in WT mouse kidney after 14 days of UUO. Overlay pictures were obtained by sequential immunostaining technique as described in Material and methods. Co-localization of murine S100A8/A9 are shown in yellow. Triple overlay is shown in pink/purple colour and indicated with pink arrows (S100A8, S100A9 and LY6G) (magnification ×40). Graph data are mean ± standard error of the mean (s.e.m.). #$P < 0{\cdot}05$ *versus* WT at the same time-point, *$P < 0{\cdot}05$, **$P < 0{\cdot}005$, ***$P < 0{\cdot}0005$ *versus* CL unobstructed kidney. Scale bar 200 μm; $n = 3$ for human data. For statistical analysis of murine data the Mann–Whitney U-test was used for comparison between two groups; $n = 7/8$ mice per group.

Fremont, CA, USA) was added to the cells prior to acquisition. Cells were acquired on a fluorescence activated cell sorter (FACS)Canto (Becton Dickinson, San Jose, CA, USA) and analysed with Flow-Jo software (TreeStar, Inc., Ashland, OR, USA).

The activity of caspase-3 was measured in cell lysates, using the fluorogenic substrate Ac-DEVD-AMC (Enzo Life Sciences, Exeter, UK), in the caspase assay buffer [HEPES 20 mM, dimethyl [3-(propyl)] azaniumyl propane-1-sulphonate (CHAPS) 5 mM, dithiothreitol (DTT) 5 mM, EDTA 5 mM]. Fluorescence was measured with a 360-nm excitation wavelength and 460-nm emission wavelength.

For immunofluorescence on MDCK cells cultured on coverslips, cells were fixed and permeabilized before incubation with primary antibodies followed by AlexaFluor 488-conjugated secondary antibody. Pictures were taken with a fluorescence light microscope (Leica; magnification ×40).

Statistics

Comparisons between two groups were analysed using the Mann–Whitney *U*-test or between more than two groups with the Kruskal–Wallis test, unless mentioned otherwise in the figure legend. For *in-vitro* experiments, comparison between two groups was analysed using the two-tailed Student's *t*-test. Values are expressed as mean ± standard error of the mean (s.e.m.). *P*-values < 0·05 were considered statistically significant.

Results

Increased S100A8/A9 expression in human biopsies and murine renal tissue with obstructive nephropathy

We first investigated the expression of S100A8 and S100A9 in renal biopsies of patients with obstructive hydronephrosis. As a control we used the healthy area in renal tissue derived from nephrectomy for malignancy. Using immunohistochemistry (IHC) we observed that S100A8 and S100A9 expression is increased during obstructive nephropathy and is localized to the tubulo-interstitial compartment (Fig. 1a). It is noteworthy that non-myeloid cells such as tubular cells did not show any positivity for S100A8/A9 as described previously after stress conditions [8]. The S100A8/A9-positive cells were identified as granulocytes and not macrophages, as displayed by co-localization (overlay displayed in yellow and highlighted with arrow) of S100A8/A9 (red) with CD15 (green), a marker for granulocytes but not with CD68 (macrophage marker: blue) (Fig. 1b).

Next, we evaluated expression and localization in the experimental model of obstructive nephropathy UUO, which mimics the various stages of progressive renal injury and fibrosis [25]. Similar to human staining, in murine kidney we detected S100A8- and S100A9- positive cells mainly within the interstitial compartment (Fig. 1c). Digital quantification of stained tissue revealed an increased expression of S100A8/A9 over time (Fig. 1d,e). Staining for S100A8 was almost undetectable in S100A9 KO mice (Fig. 1c,e). As S100A8/A9 functions as a heterodimer, we measured this by enzyme-linked immunosorbent assay (ELISA). S100A8/A9 complex is expressed significantly 14 days after surgery, compared to contralateral tissue (Fig. 1f).

As in the human study, sequential immunostaining was used to determine the cellular source of S100A8/A9 expression in kidney post-UUO at day 14. We found that S100A8 (red) co-localizes with S100A9 (green) (overlay in yellow) suggesting that the functional heterodimer is present. Moreover, and in line with human data, the complex co-localizes with the granulocyte marker Ly6G (blue) (overlay: pink positive cells highlighted with pink arrow) but not with the macrophage marker F480 (blue) (Fig. 1g). Of note, staining for granulocyte influx (Ly6G) in renal tissue was similar between WT and S100A9 KO mice 1 and 14 days following UUO (WT *versus* S100A9

KO mice, day 1: 1·1 ± 0·3 *versus* 1.9 ± 0·4 and day 14: 7 ± 1·8 *versus* 8·6 ± 4·4% positive staining/HPF). The small percentage of S100A8/A9-positive cells, which do not express the Ly6G marker, appears to be positive for DBA but not for LTL (Supporting information, Fig. S1). Together, these human and experimental data suggest a potential role for S100A8/A9 in progressive renal injury.

S100A9 deficiency dampens renal fibrosis independently of leucocyte infiltration

To directly assess the contribution of S100A8/A9 to renal interstitial fibrosis, we analysed the presence of α-SMA-positive myofibroblasts and collagen deposits in WT and S100A9 KO mice after UUO. We have described previously that, in untreated conditions, levels of α-SMA, collagen-1 and macrophage polarization markers were similar between WT and KO mice [21].

Differences were found at time-points where we observed the highest expression of the S100A8/A9 monomer (such as days 7 and 14). We did not detect any differences in these parameters at days 1 and 3 following UUO (data not shown). Seven days following UUO, kidneys of S100A9 KO mice showed less accumulation of myofibroblasts compared to WT mice, whereas no differences were observed at day 14 (Fig. 2a). A reduction of collagen deposition, detected by IHC, was observed in S100A9 KO mice compared to WT at 7 and 14 days of UUO (Fig. 2b). The latter finding was also verified by PSR staining, which confirmed that KO mice have reduced collagen deposits 14 days post-UUO (Fig. 2c).

The reduced extent of fibrosis in the S100A9 KO animals also affected the expression of the profibrotic growth factor platelet-derived growth factor (*Pdgfa*) and collagen-1 genes (*col1a1*), particularly 14 days after UUO (Fig. 2d,e). During progression of fibrosis, particularly 14 days upon UUO, TGF-β1 is expressed and activated in WT mice, whereas in S100A9 KO animals appears to be significantly decreased (Fig. 2f). The rescue in renal fibrosis was accompanied by a functional renal improvement, as shown by decreased levels of creatinine (Fig. 2g).

Sustained inflammation is a hallmark of progressive renal fibrosis [3]. In particular, macrophages modulate tubulo-interstitial damage after UUO [26]. Accumulation of F4/80$^+$ macrophages and the transcript expression of proinflammatory mediators such as C-C motif chemokine ligand 2 (CCL2), interleukin (IL)-6 and tumour necrosis factor (TNF)-α was comparable between WT and S100A9 KO mice at days 7 and 14 post-UUO (Fig. 3a–d). S100A8/A9 can modulate macrophage polarization [21,27]. However, we found no differences in the expression of M1- and M2-differentiated macrophages markers (*Nos2*, *Irf5*, *Ly6c* and *Arg1*, *Irf4* and *Mrc1*, respectively) between WT and KO mice (Fig. 3e,f).

Altogether, these results suggest that S100A8/A9 has a detrimental effect on the development of UUO-induced renal fibrosis, which was not associated with a difference in inflammatory cytokine response or modulation of gene expression, indicative of macrophage polarization.

S100A9 deficiency preserves tubular epithelial cells integrity following UUO

Next, we evaluated whether differences in fibrosis between WT and S100A9 KO mice could be ascribed to an effect on TECs injury. Thus, we analysed TECs apoptosis, proliferation and morphology at days 7 and 14 post- UUO. Compared to WT mice, S100A9 KO mice display decreased tubular apoptosis, as shown by cleaved caspase-3 positive tubular cells (Fig. 4a,d). In addition, the proliferation of tubular cells, as verified by Ki67 positivity, was increased in S100A9 KO mice compared to WT animals (Fig. 4b,e). These findings were corroborated by the presence of an increased number of intact tubules in S100A9 KO mice, as detected by the presence of brush border and regular morphology with PAS-D staining (Fig. 4c,f). Epithelial mesenchymal transition (EMT) occurs in TECs in response to injury and can lead to the progression of tubulo-interstitial fibrosis [3,25]. Critical molecular events in EMT are characterized by loss of expression of adhesion molecule E-cadherin and by the induction of the transcription factor Twist [28]. Compared to WT mice, S100A9 KO mice display increased expression of the E-cadherin transcript 14 days post-surgery (Fig. 4g). E-cadherin expression is regulated negatively by Twist, which was decreased in S100A9 KO animals compared to WT upon 14 days of UUO (Fig. 4h). Given the decreased activation of the key transition steps leading to EMT, together with the development of fibrosis, we investigated whether these observations correlated with the level of renoprotective cytokine IL-10, shown recently to have anti-fibrotic effects in the context of UUO [29]. Indeed, IL-10 was increased significantly in S100A9 KO mice compared to WT 14 days after UUO (Fig. 4i). Altogether, these data suggest that S100A9 deficiency ameliorates renal fibrosis by preserving tubular health, possibly via the suppression of critical molecular events in EMT.

S100A9 deficiency is associated with down-regulation of RAGE and its interacting receptor ICAM-1

S100A8/A9 can bind either TLR-4 or RAGE receptors, which are both up-regulated in epithelial cells following UUO [17]. We therefore analysed and normalized the expression of TLR-4 and RAGE protein in murine kidneys of WT and S100A9 KO mice 14 days post-UUO,

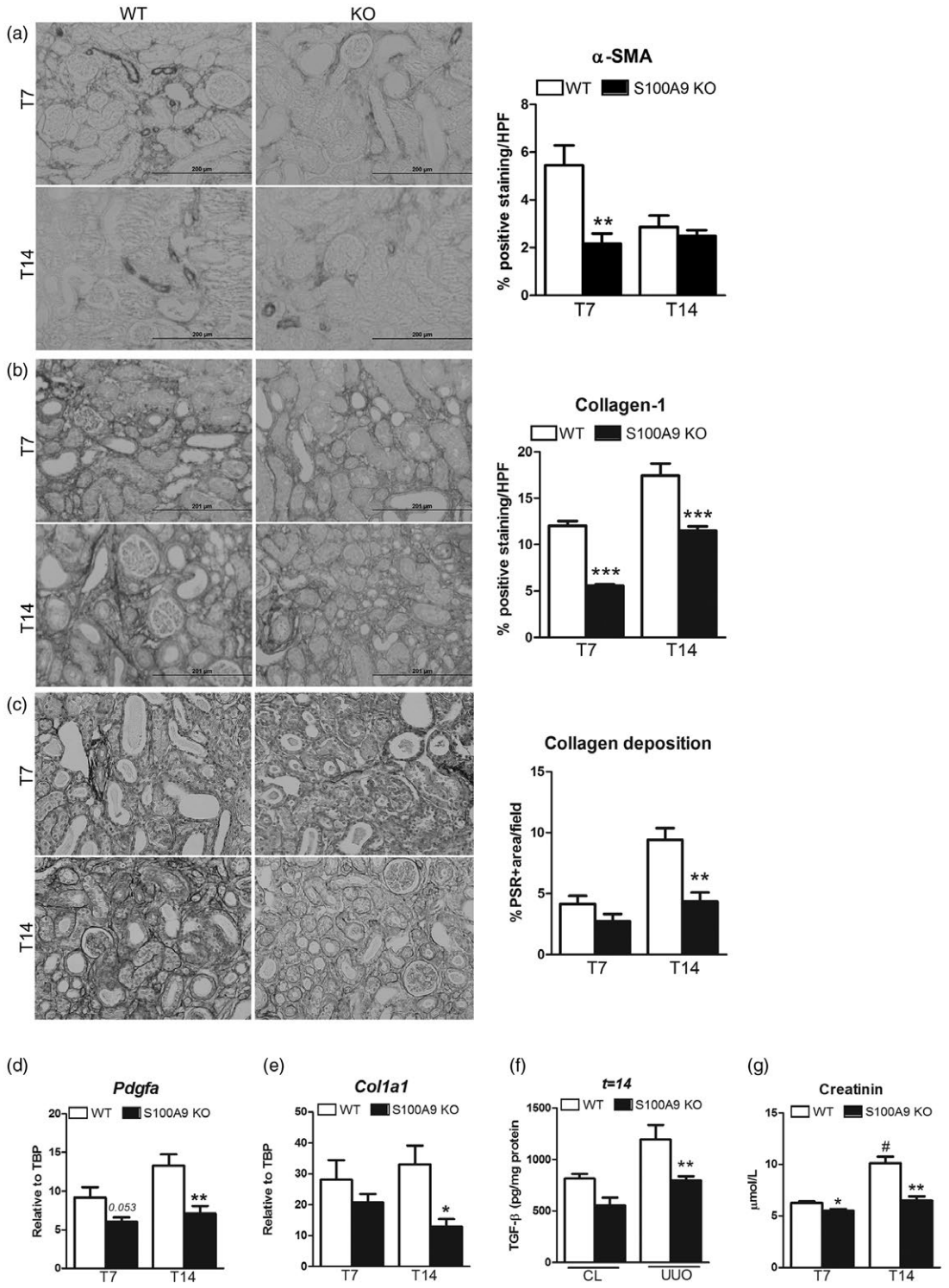

Fig. 2. Renal fibrosis in wild-type (WT) and S100A9 knock-out (KO) mice during unilateral ureteral obstruction (UUO). Renal fibrosis as displayed by representative pictures and quantification of (a) α-smooth muscle actin (SMA), (b) collagen 1 and (c) Picro Sirius Red (PSR) staining on renal tissue slides from WT and S100A9 KO mice 7 and 14 days after UUO. (d,e) Transcript expression of pro-fibrotic genes *Pdgfa* and Col1a1 measured by reverse transcriptase–polymerase chain reaction (RT–PCR). Data are expressed relative to the housekeeping gene *Tbp in* WT and S100A9 KO mice 7 and 14 days after UUO. (f) Transforming growth factor (TGF)-β protein detected by enzyme-linked immunosorbent assay (ELISA) in contralateral (CL) and obstructed kidney from WT and S100A9 KO mice, 14 days post-UUO. (g) Plasma levels of creatinine in WT and S100A9 KO animals, 7 and 14 days after UUO. HPF = high-power field. Magnification ×20. The Mann–Whitney *U*-test was used for comparisons between two groups; $n = 7/8$ mice per group. Graph data are mean ± standard error of the mean (s.e.m.). $^{*}P < 0{\cdot}05$, $^{**}P < 0{\cdot}005$, $^{***}P < 0{\cdot}0005$ *versus* WT at the same time-point. $\#P < 0{\cdot}005$ compared to WT at T7. Scale bar 200 µm.

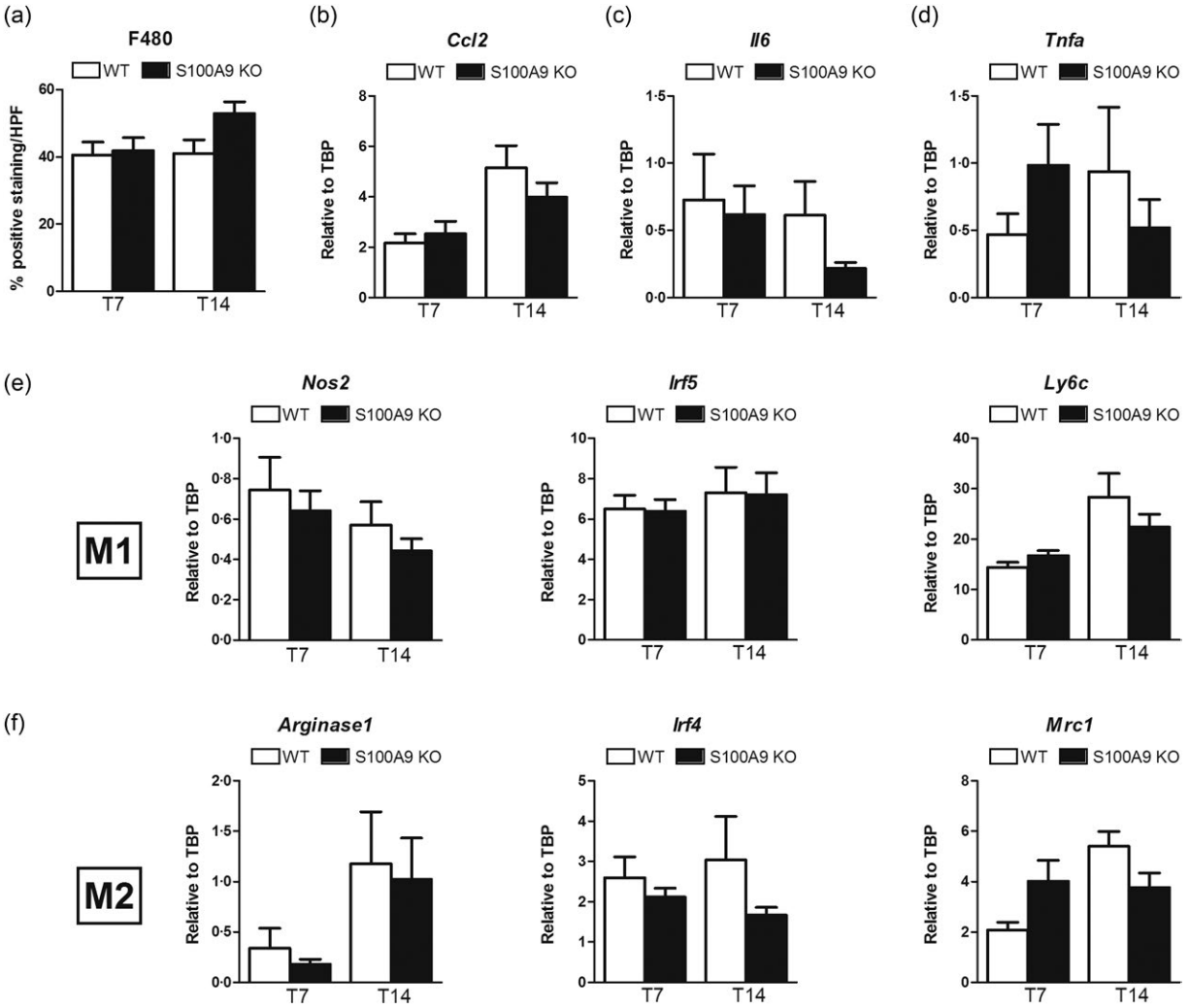

Fig. 3. Inflammatory parameters in WT and S100A9 KO mice. (a) Renal macrophages accumulation shown as percentage of F480 positive area detected by IHC, in renal tissues 7 and 14 days post- unilateral ureteral obstruction (UUO). Next, transcript expression in renal tissue of (b) *Ccl2* (the gene for MCP-1), (c) *Il6* and (d) *Tnfa* measured by reverse transcriptase–polymerase chain reaction (RT–PCR). (e) Transcript expression in renal tissue of M1 markers, *Nos2*, *Irf5*, *Ly6c* and (f) M2 macrophage markers, *Arginase-1, Irf4, Mrc1* measured by reverse transcription–polymerase chain reaction (RT–PCR). Values are relative to the housekeeping gene *Tbp*. Data are expressed as mean ± standard error of the mean (s.e.m.); $n = 7/8$ samples per group.

as more consistent results were obtained at this time-point. TLR-4 and RAGE proteins showed a similar down-regulated pattern in kidney lysates after UUO in the absence of S100A9, with statistical significance for RAGE (Fig. 5a–c).

As, together with intracellular adhesion molecule-1 (ICAM-1), RAGE may mediate interstitial fibrosis by modulating epithelial integrity during UUO [17], we investigated the expression of ICAM-1. Our results show that besides RAGE, ICAM-1 is also reduced in KO kidneys 14 days post-UUO compared to WT tissue at mRNA and protein levels (Fig. 5d,e). It is conceivable that the S100A8/A9 may induce tubular injury via RAGE and its interacting receptor ICAM-1.

Recombinant S100A8/A9 directly affects TECs de-differentiation and cell death *in vitro*

In order to unravel the mechanism by which S100A8/A9 contributes to tubular injury, TECs were stimulated with different concentrations of recombinant S100A8/A9 protein. As previous studies have shown that S100A8/A9 impairs endothelial cell integrity by down-regulation of cell junction protein [30,31], which leads to cell death, we measured the expression of cell junction protein zonula occludens-1 (ZO-1) and adhesion molecule E-cadherin in TECs stimulated with a low concentration of S100A8/A9. Our results show that S100A8/A9 induces a profound down-regulation of ZO-1 protein expression and a trend

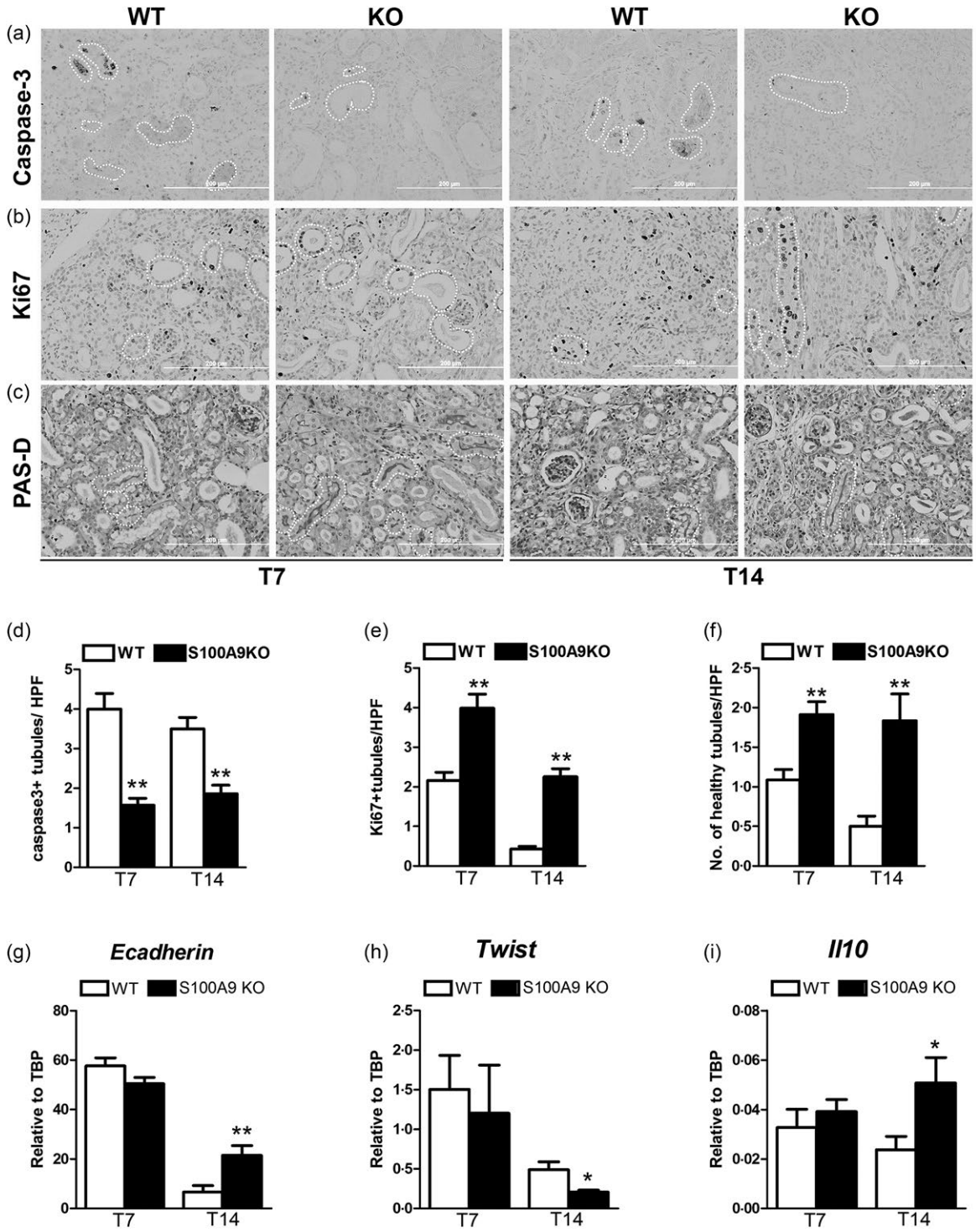

Fig. 4. Tubular injury and epithelial mesenchymal transition (EMT) in wild-type (WT) and S100A9-deficient mice, 7 and 14 days post-unilateral ureteral obstruction (UUO). (a,d) Tubular apoptosis as displayed by representative pictures and quantification of cleaved caspase-3 positive tubules on renal tissue slides from WT and S100A9 knock-out (KO) mice. (b,e) Tubular proliferation as displayed by representative pictures and quantification of Ki-67. No interstitial Ki-67-positive cells were included in the count. (c,f) Periodic acid–Schiff-diastase (PAS-D) staining of renal tissue was used to quantify the number of healthy tubules (by presence of brush border) in WT and S100A9 KO mice 7 and 14 days after UUO. Only tubules surrounding glomeruli were considered for the above analysis. White drawing in the pictures show an example of tubular cells included in the count. The number of caspase-3, Ki67-positive and healthy tubular epithelial cells (TECs) (measured by PAS-D) were counted in 10 non-overlapping high-power fields (HPFs), having glomerular cells as reference, in a blind manner, with a ×40 magnification. (g–i) Transcript expression of *E-cadherin*, *Twist* and *Il10* measured by reverse transcriptase–polymerase chain reaction (RT–PCR) in WT and S100A9 KO, 7 and 14 days upon UUO. Values are normalized to the housekeeping gene Tbp. The Mann–Whitney *U*- test was used for comparison between two groups; $n = 7/8$ mice per group. Graph data are expressed as mean ± standard error of the mean (s.e.m.). $^{*}P < 0{\cdot}05$, $^{**}P < 0{\cdot}005$, *versus* WT at the same time-point. Scale bar 200 μm.

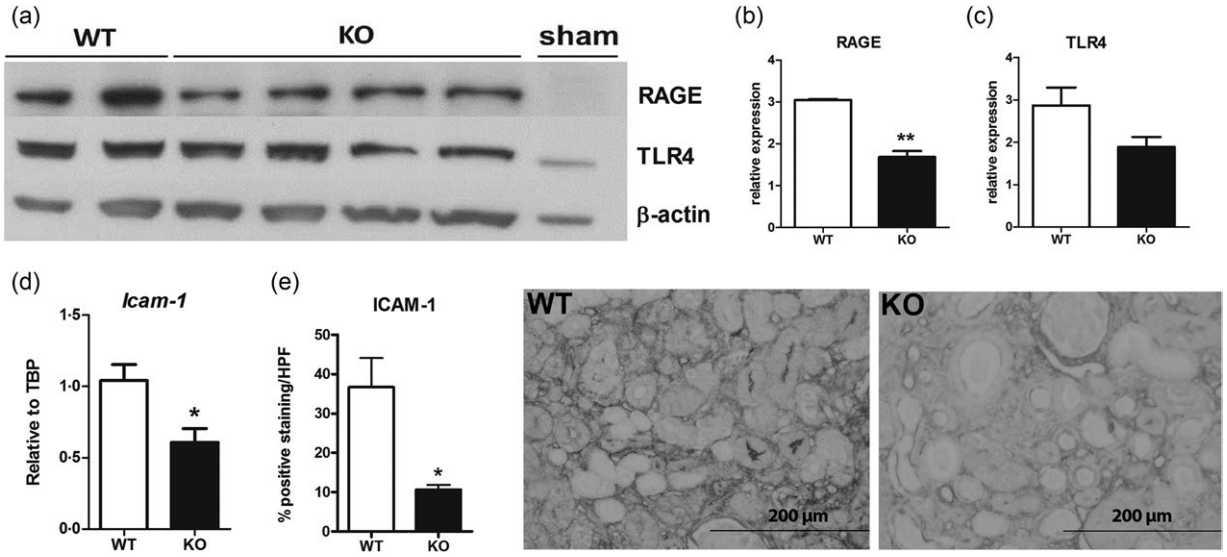

Fig. 5. Expression of S100A8/A9 receptors, Toll-like receptor (TLR)-4 and receptor for advanced glycation end-products (RAGE). (a–c) Expression of RAGE and TLR-4 protein measured by Western blot. Quantification of RAGE and TLR-4 in wild-type (WT) ($n = 2$) and knock-out (KO) ($n = 4$) kidney lysates from day 14 after unilateral ureteral obstruction (UUO). Values were normalized to the levels of β-actin. Statistical difference were analysed by two-tailed Student's *t*-test. (d,e) Intercellular adhesion molecule 1 (ICAM-1) transcript and protein expression as measured by reverse transcriptase–polymerase chain reaction (RT–PCR)and immunohistochemistry (IHC), respectively, in tissue of WT and KO mice, 14 days after UUO; $n = 5$ mice per group. (e) Representative pictures of ICAM-1 IHC. Percentage of positive staining was measured by ImageJ software. The Mann–Whitney *U*-test was used for comparison between these groups. Graph data are mean ± standard error of the mean (s.e.m.). $^*P < 0{\cdot}05$, $^{**}P < 0{\cdot}005$ *versus* WT. Scale bar 200 µm.

in E-cadherin decrease, which was also confirmed in a polarized cellular system of TECs (Fig. 6a and Supporting information, Fig. S2). Moreover, rS100A8/A9 affects not only cell–cell junction, but the expression of mitotic cyclin B1 (Fig. 6a), the latter suggesting a proliferation arrest. Of note, the cell-cycle arrest did not induce full EMT in TECs, measured by expression of α-SMA (data not shown).

To study whether extracellular S100A8/A9 can affect cell death, TECs were stimulated with increasing concentrations of rS100A8/A9 and apoptosis/necrosis was measured by FACS analysis with annexin V/PI staining. S100A8/A9 induced late apoptosis/necrosis in TECs, as shown by an increased percentage of PI/annexin V^+ cells in a concentration-dependent manner (Fig. 6b). This cytotoxic effect of S100A8/A9 was not reversed by treatment with a Pan-caspase inhibitor Q-VD-OPh hydrate (QVD), suggesting that S100A8/A9 induces a caspase-independent cell death, most probably necrosis, as observed by PI uptake (Fig. 6c). In support of this observation, we found that caspase-3 activity was not affected by incubation with rS100A8/A9 or upon ligand activation of TLR-4 or RAGE receptor (Supporting information, Fig. S3).

However, to further mimic a UUO-like model *in vitro*, we co-stimulated cells with rTGF-β1 and rS100A8/A9 and evaluated the effect on TEC cell death. Surprisingly, we noticed that the fibrotic trigger in combination with S100A8/A9 leads to increased early apoptosis and not necrosis, as observed by increased annexin V^+ cells (Fig. 6d).

Altogether, these *in-vitro* data indicate that S100A8/A9 induces polarity changes in TECs which might disrupt the interaction between epithelial cells, driving subsequent cell death and tubular atrophy during progressive renal fibrosis.

Discussion

CKD is a pathological condition with different aetiologies characterized by a progressive loss of nephrons and renal fibrosis. Treatments to prevent renal fibrosis still rely upon regimes targeting the underlying disease processes, such as diabetes and hypertension [1]. Identifying novel targets which delay, arrest or reverse the progression of tissue fibrosis may lead to treatment opportunities for patients suffering from CKD. Increasing evidence suggests that DAMPs released during tissue injury, together with the innate immune receptors involved in their recognition [9], contribute to the development of renal fibrosis [10,11]. However, the role of the damage molecule S100A8/A9 in the pathogenesis of obstructive nephropathy has not yet been unravelled. This study provides evidence that S100A8/A9 protein may emerge as a target for novel therapeutic interventions to preserve parenchymal integrity

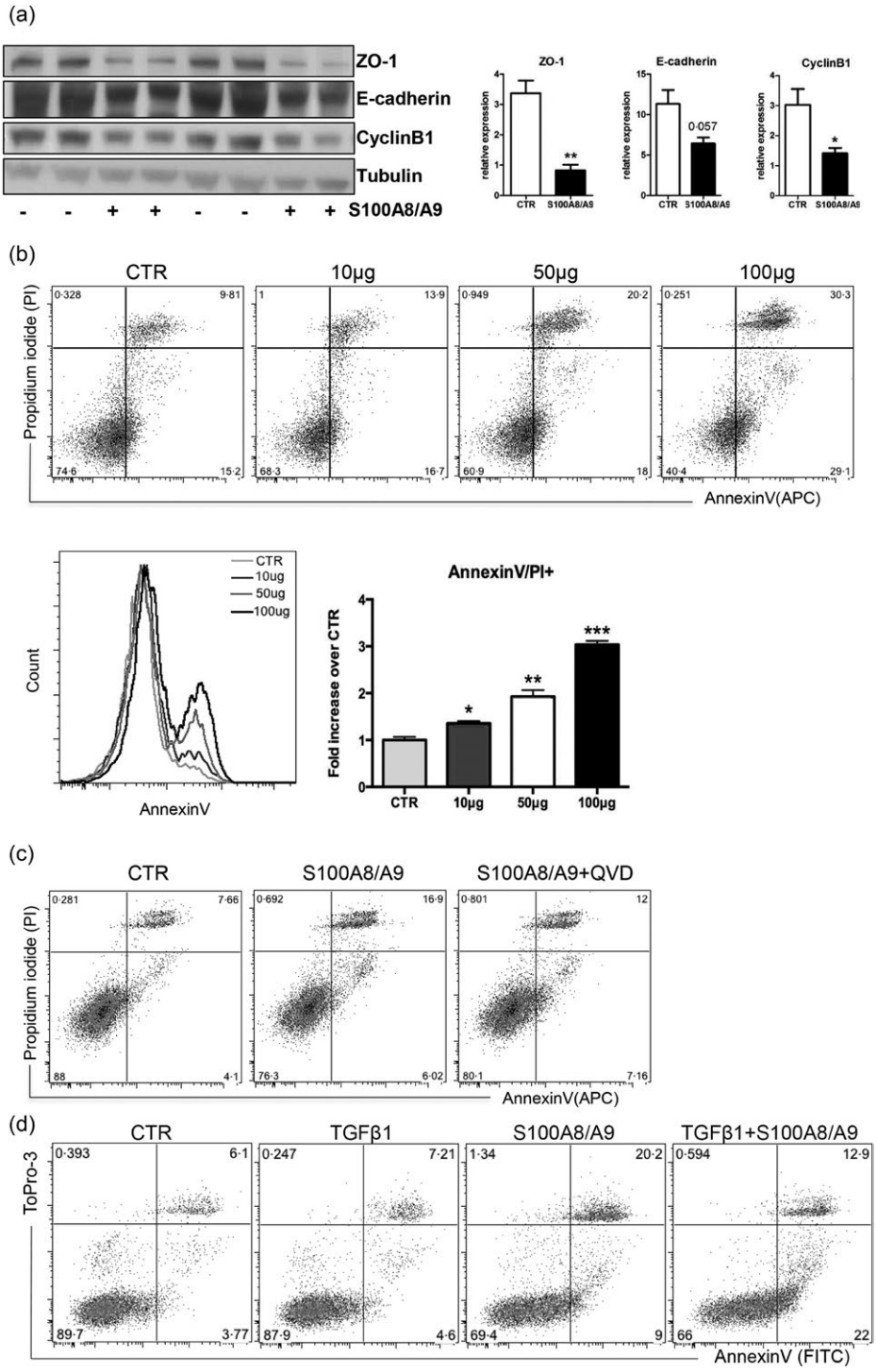

Fig. 6. Effect of extracellular S100A8/A9 on tubular epithelial cells. (a) Western blot analysis of primary tubular epithelial cells (TECs) isolated from four wild-type WT) mice (Charles River) and stimulated with a low concentration of rS100A8/A9 (5 µg/ml) for 24 h in HK2 medium. Protein expression of ZO-1, E-cadherin and cyclin B1 are calculated relatively to the levels of tubulin. (b) Fluorescence activated cell sorter (FACS) plots and histograms relative to cell death measured by annexin V/propidium iodide (PI) staining in stimulated immortalized proximal TEC (IM-PTEC) cells with S100A8/A9 (10, 50 and 100 µg/ml) for 24 h in hexokinase 2 (HK2) medium. The percentage of late apoptotic cells/necrotic (double-positive) are showed in the graph. (c) Representative plots of IM-TEC stimulated with S100A8/A9 (50 µg/ml) in the presence or absence of the Q-VD-OPh hydrate (ApexBio), a pan-caspase inhibitor (20 µM). (d) Representative plots of IM-TEC stimulated with rS100A8/A9 (100 µg/ml) and/or recombinant human transforming growth factor (rhTGF)-β1 (20 ng/ml). Cells were treated for 24 h and harvested for annexin V/PI or To-Pro3 staining. FACS data are representative of three independent experiments. Statistical difference were analysed by two-tailed Student's *t*-test. Data are expressed as mean ± standard error of the mean (s.e.m.). $^{*}P < 0{\cdot}05$, $^{**}P < 0{\cdot}005$, $^{***}P < 0{\cdot}0005$ versus unstimulated control.

as chronic fibrotic disease progresses. We found that S100A8/A9 mediates renal fibrosis, activation of critical molecular events in EMT and tubular apoptosis independently of leucocyte infiltration in the kidney after UUO. *In vitro*, we showed that S100A8/A9 has a deleterious effect on TEC morphology, by inducing loss of cell junction proteins and arrest of cell proliferation, possibly driving subsequent irreversible tubular damage. These changes in tubular morphology result eventually in cell death by apoptosis, when S100A8/A9 is combined with a pro-fibrotic trigger such as TGF-β1.

S100A8/A9 is a critical player during inflammatory responses [32]. Previous studies have shown that, in human diseases, S100A8/A9 can be detected in serum, aspirates or faeces of patients with rheumatoid arthritis [33], acute rejection [34,35], inflammatory bowel disease [36], lung disease [37], systemic sclerosis [38] and atherosclerosis [39]. In the context of renal fibrosis, we are the first to show that S100A8/A9 expression is increased in patients with obstructive nephropathy and localizes uniquely to interstitial granulocytes and not to other parenchymal cells, such as epithelial cells [40]. These human findings were corroborated by the experimental data where we observed increased expression of S100A8/A9 in WT mice following UUO, and its localization was similar to that observed in human samples. Despite similar experimental conditions, Fujiu *et al.* [27], showed that S100A8/A9 expression is high in collecting duct cells and that expression peaks at day 1 post-UUO, whereas in our experiment S100A8/A9 seems to be expressed mainly by granulocytes and only with a low percentage in collecting duct cells, with a peak at day 14 post-UUO. These contrasting results may be related to differences in the technical method used to identify these cells. We performed immunohistochemical staining, whereas Fujiu *et al.* looked at the transcript expression of sorted cells from UUO kidney. The results of two techniques may not be fully comparable, as protein and mRNA might have discordant results in similar pathological conditions [41].

Although we detected S100A8/A9 expression mainly on infiltrating granulocytes, mice lacking S100A9 displayed similar granulocyte numbers compared to WT mice, as shown previously by our group in the acute model of injury [21], suggesting a limited role of S100A8/A9 in granulocyte infiltration in both acute and chronic models of renal injury. Nonetheless, the role of granulocytes in the progression of renal fibrosis is not as pronounced as the role of macrophages [42]. Instead, the latter play a pivotal role in the development of tubulo-interstitial injury, due to the activation of an excessive inflammatory response [26,43]. Previously, in renal ischaemia reperfusion (IR), we showed a beneficial role of S100A8/A9 in controlling macrophage-mediated renal repair by preventing excessive M2 polarization and renal fibrosis [21]. Supporting this study, Rekers *et al.* showed that high levels of S100A8/A9 correlated with improved graft outcome after kidney transplantation [35]. Thus, we hypothesized that S100A8/A9 would dampen macrophage-induced inflammation and the development of renal fibrosis following UUO. Surprisingly, in sharp contrast to the results obtained in renal IR and allograft rejection, we found that S100A9 KO mice were protected against renal fibrosis, independently of the activation of the inflammatory response, macrophage infiltration and polarization, which suggests a deleterious role for S100A8/A9 in renal fibrogenesis.

In the UUO model, one study demonstrated that Klf5 controls macrophage polarity via S100A8/A9, thereby controlling tissue remodelling and limiting fibrosis [27]. These findings were obtained in mice aploinsufficient for Klf5 which, although not specific for S100A8/A9, is known to regulate other cellular processes such as growth and differentiation [27]. Apparently, S100A8/A9 is a beneficial player in the progression of acute renal disease, but shows contrasting results in the context of obstructive nephropathy. We speculate that in the renal IR model the functional S100A8/A9 signalling in non-parenchymal cells is necessary to recognize the initial damage from ischaemic cells and initiate a proper wound-healing response from macrophages. Indeed, the aberrant innate immune response observed in the KO animals after IR may be responsible for an altered wound-healing process with progression to renal fibrosis.

If S100A8/A9 protein reduces the risk of maladaptive renal repair following renal IR, low levels of the protein during the progression of renal fibrosis may prevent perpetuation to irreversible damage. This dual role of S100A8/A9 might be dependent upon the primary insult driving the progression of renal fibrosis. In the UUO model, S100A8/A9 signalling in immune cells seems to be dispensable for the progression of renal fibrosis, as demonstrated in mice over-expressing S100A12/A8/A9 specifically in myeloid cells and subjected to UUO ligation. These mice displayed no differences in interstitial inflammation and fibrosis/tubular atrophy in the kidney, suggesting a dispensable role for inflammatory cell-associated S100A8/A9 in renal fibrosis [44]. Interestingly, similar to our study, a study on cardiac fibrosis, showed that inhibition of S100A8/A9 via a neutralizing antibody suppressed angiotensin II (AngII)-induced perivascular and interstitial fibrosis [45].

This would suggest that, in the absence of S100A8/A9, other DAMPs are released during chronic damage which

may compensate for the activation of the inflammatory response. S100A8/A9 signals via RAGE and TLR-4. Mice deficient for both receptors show a phenotype similar to that of S100A9 KO mice, namely decreased fibrosis independently of leucocyte infiltration and reduced nuclear factor kappa B (NF-κB) activation [17]. Thus, it appears that S100A8/A9 and its interacting receptors modulate the extent of fibrosis via pathological mechanisms activated in parenchymal cells, instead of regulating the inflammatory response [46]. Hence, blocking DAMPs might be a great alternative for targeting the multiple receptors associated with immunopathology, as it will not hinder pathogen detection.

Following UUO, TECs become injured and start to lose their functionality. As a survival mechanism, TECs start an EMT programme with myofibroblast recruitment and subsequent collagen deposits [2,47]. S100A9 KO mice displayed decreased recruitment of myofibroblasts, collagen deposits and pro-fibrotic mediators, suggesting that injury was contained in TECs, as the inflammatory compartment was unaffected. Indeed, S100A9KO mice displayed improved renal function and decreased tubular injury, which resulted in decreased activation of critical EMT steps in TECs. Among S100A8/A9 receptors, RAGE and its interacting receptor ICAM-1 have been shown to mediate renal fibrosis via the loss of epithelial cell integrity and by modulating cellular apoptosis [17]. Other members of the S100 family are known to trigger cell death in cancer cells by binding to RAGE [48]. Expression of RAGE and its interacting receptor ICAM-1 was dampened in the absence of S100A9 after UUO. However, more experiments are needed to ascertain whether S100A8/A9-mediated tubular injury and renal fibrosis may be dependent upon the RAGE-ICAM-1 interaction. Our data argue in favour of a possible involvement.

Finally, we explored the mechanism by which S100A8/A9 may contribute to tubular injury and fibrosis. We found that tubular epithelial cell lines stimulated with low concentrations of rS100A8/A9 displayed down-regulation of tight junction protein ZO-1 and adhesion molecule E-cadherin, together with cell-cycle arrest. Extracellular S100A8/A9 can affect cell growth and have cytotoxic/apoptotic effects on different cell types in a dose-dependent manner [30,31,49,50]. Our results are in unison with these studies, as a high concentration of rS100A8/A9 induced a caspase-independent cell death in TECs, most probably necrosis. However when rS100A8/A9 is combined with a pro-fibrotic trigger, tubular apoptosis is pronounced. Increasing evidence describes a relationship between cell-cycle arrest and renal fibrosis [51]. The reduction of fibrosis observed in S100A9 KO mice may be explained partially by the decreased tubular apoptosis and destruction.

We believe that treatment with recombinant protein induces dissolution of the cell–cell junction, which is essential for maintaining tubular structure and may lead to cell death by necrosis. Consistent with our results, S100A8/A9 was shown to induce loss of endothelial cell contact which triggered subsequent cell death, not exclusively via the apoptotic pathway [30]. However, during progression of fibrosis, S100A8/A9 affects mainly tubular apoptosis, as confirmed *in vivo* and *in vitro*.

In conclusion, our study demonstrates that S100A8/A9 mediates tubular apoptosis and renal fibrosis presumably through the loss of TECs contacts and activation of EMT transition steps. Targeting the TLR-4 and RAGE shared ligand, S100A8/A9, could be a therapeutic strategy to halt renal fibrosis and parenchymal damage in patients with CKD.

Acknowledgements

The authors would like to acknowledge Angelique Scantlebery for proof-reading the paper. This work was supported further by the Dutch Kidney Foundation and the Netherlands Organization for Health Research and Development (ZonMw) to M. D. (Meer Kennis met Minder Dieren; no. 114024040) and J. C. L. (Vidi #91712386), (ASPASIA no. 015.008.044).

Disclosure

The authors declare no potential conflicts of interest to disclose.

References

1 Rockey DC, Bell PD, Hill JA. Fibrosis: a common pathway to organ injury and failure. N Engl J Med 2015;**372**:1138–49.
2 Lovisa S, LeBleu VS, Tampe B *et al*. Epithelial-to-mesenchymal transition induces cell cycle arrest and parenchymal damage in renal fibrosis. Nat Med 2015;**21**:998–1009.
3 Lovisa S, Zeisberg M, Kalluri R. Partial epithelial-to-mesenchymal transition and other new mechanisms of kidney fibrosis. Trends Endocrinol Metab 2016;**27**:681–95.
4 Vogl T, Ludwig S, Goebeler M *et al*. MRP8 and MRP14 control microtubule reorganization during transendothelial migration of phagocytes. Blood 2004;**104**:4260–8.
5 Lackmann M, Rajasekariah P, Iismaa SE *et al*. Identification of a chemotactic domain of the pro-inflammatory S100 protein CP-10. J Immunol. 1993;**150**:2981–91.
6 Simard J-C, Cesaro A, Chapeton-Montes J *et al*. S100A8 and S100A9 induce cytokine expression and regulate the NLRP3 inflammasome via ROS-dependent activation of NF-κB1. PLOS ONE 2013;**8**:e72138.

7 Donato R. Intracellular and extracellular roles of S100 proteins. Microsc Res Tech 2003;**60**:540–51.

8 Donato R, Cannon BR, Sorci G *et al*. Functions of S100 proteins. Curr Mol Med 2013;**13**:24–57.

9 Matzinger P. Tolerance, danger, and the extended family. Annu Rev Immunol 1994;**12**:991–1045.

10 Leemans JC, Kors L, Anders H-J, Florquin S. Pattern recognition receptors and the inflammasome in kidney disease. Nat Rev Nephrol 2014;**10**:398–414.

11 Anders H-J, Schaefer L. Beyond tissue injury-damage-associated molecular patterns, toll-like receptors, and inflammasomes also drive regeneration and fibrosis. J Am Soc Nephrol 2014;**25**:1387–400.

12 Johnson GB, Brunn GJ, Platt JL. Activation of mammalian toll-like receptors by endogenous agonists. Crit Rev Immunol. 2003;**23**:15–44.

13 Vogl T, Tenbrock K, Ludwig S *et al*. Mrp8 and Mrp14 are endogenous activators of toll-like receptor 4, promoting lethal, endotoxin-induced shock. Nat Med 2007;**13**:1042–9.

14 Ehlermann P, Eggers K, Bierhaus A *et al*. Increased proinflammatory endothelial response to S100A8/A9 after preactivation through advanced glycation end products. Cardiovasc Diabetol 2006;**5**:6.

15 Narumi K, Miyakawa R, Ueda R *et al*. Proinflammatory proteins S100A8/S100A9 activate NK cells via interaction with RAGE. J Immunol 2015;**194**:5539–48.

16 Yiu WH, Lin M, Tang SCW. Toll-like receptor activation: from renal inflammation to fibrosis. Kidney Int 2014;**4**:20–5.

17 Gasparitsch M, Arndt A-K, Pawlitschek F *et al*. RAGE-mediated interstitial fibrosis in neonatal obstructive nephropathy is independent of NF-κB activation. Kidney Int 2013;**84**:911–9.

18 Pulskens WP, Rampanelli E, Teske GJ *et al*. TLR4 promotes fibrosis but attenuates tubular damage in progressive renal injury. J Am Soc Nephrol 2010;**21**:1299–308.

19 Tammaro A, Stroo I, Rampanelli E *et al*. Role of TREM1-DAP12 in renal inflammation during obstructive nephropathy. PLOS ONE 2013;**8**:e82498.

20 Passey RJ, Williams E, Lichanska AM *et al*. A null mutation in the inflammation-associated S100 protein S100A8 causes early resorption of the mouse embryo. J Immunol 1999;**163**:2209–16.

21 Dessing MC, Tammaro A, Pulskens WP *et al*. The calcium-binding protein complex S100A8/A9 has a crucial role in controlling macrophage-mediated renal repair following ischemia/reperfusion. Kidney Int 2015;**87**:85–94.

22 Stokman G, Kers J, Yapici Ü *et al*. Predominant tubular interleukin-18 expression in polyomavirus-associated nephropathy. Transplantation 2016;**100**:e88–95.

23 Pulskens WP, Teske GJ, Butter LM *et al*. Toll-like receptor-4 coordinates the innate immune response of the kidney to renal ischemia/reperfusion injury. PLOS ONE 2008;**3**:e3596.

24 Stokman G, Qin Y, Genieser H-G *et al*. Epac-rap signaling reduces cellular stress and ischemia-induced kidney failure. J Am Soc Nephrol 2011;**22**:859–72.

25 Bascands J-L, Schanstra JP. Obstructive nephropathy: insights from genetically engineered animals. Kidney Int 2005;**68**:925–37.

26 Meng X-M, Nikolic-Paterson DJ, Lan HY. Inflammatory processes in renal fibrosis. Nat Rev Nephrol 2014;**10**:493–503.

27 Fujiu K, Manabe I, Nagai R. Renal collecting duct epithelial cells regulate inflammation in tubulointerstitial damage in mice. J Clin Invest 2011;**121**:3425–41.

28 Lamouille S, Xu J, Derynck R. Molecular mechanisms of epithelial-mesenchymal transition. Nat Rev Mol Cell Biol 2014;**15**:178–96.

29 Jin Y, Liu R, Xie J, Xiong H, He JC, Chen N. Interleukin-10 deficiency aggravates kidney inflammation and fibrosis in the unilateral ureteral obstruction mouse model. Lab Invest 2013;**93**:801–11.

30 Viemann D, Barczyk K, Vogl T *et al*. MRP8/MRP14 impairs endothelial integrity and induces a caspase-dependent and -independent cell death program. Blood 2007;**109**:2453.

31 Viemann D, Strey A, Janning A *et al*. Myeloid-related proteins 8 and 14 induce a specific inflammatory response in human microvascular endothelial cells. Blood 2005;**105**:2955–62.

32 Pruenster M, Vogl T, Roth J, Sperandio M. S100A8/A9: From basic science to clinical application. Pharmacol Ther 2016;**167**:120–31.

33 Perera C, McNeil HP, Geczy CL. S100 Calgranulins in inflammatory arthritis. Immunol Cell Biol 2010;**88**:41–9.

34 Eikmans M, Roos-van Groningen MC, Sijpkens YW *et al*. Expression of surfactant protein-C, S100A8, S100A9, and B cell markers in renal allografts: investigation of the prognostic value. J Am Soc Nephrol 2005;**16**:3771–86.

35 Rekers NV, Bajema IM, Mallat MJK *et al*. Beneficial immune effects of myeloid-related proteins in kidney transplant rejection. Am J Transplant 2016;**16**:1441–55.

36 Ikhtaire S, Shajib MS, Reinisch W, Khan WI. Fecal calprotectin: its scope and utility in the management of inflammatory bowel disease. J Gastroenterol 2016;**51**:434–46.

37 Kuipers MT, Vogl T, Aslami H *et al*. High levels of S100A8/A9 proteins aggravate ventilator-induced lung injury via TLR4 signaling. PLOS ONE 2013;**8**:e68694.

38 Xu X, Wu W, Tu W *et al*. Increased expression of S100A8 and S100A9 in patients with diffuse cutaneous systemic sclerosis. A correlation with organ involvement and immunological abnormalities. Clin Rheumatol. 2013;**32**:1501–10.

39 Xu X, Wu W-y, Tu W-z *et al*. S100A8 and S100A9 in cardiovascular biology and disease. Arterioscler Thromb Vasc Biol 2013;**32**:1501–229.

40 Henke MO, Renner A, Rubin BK, Gyves JI, Lorenz E, Koo JS. UP-regulation of S100A8 and S100A9 protein in bronchial epithelial cells by lipopolysaccharide. Exp Lung Res 2006;**32**:331–47.

41 Chen G, Gharib TG, Huang C-C *et al*. Discordant protein and mRNA expression in lung adenocarcinomas. Mol Cell Proteomics 2002;**1**:304–13.

42 Höchst B, Mikulec J, Baccega T *et al*. Differential induction of Ly6G and Ly6C positive myeloid derived suppressor cells in chronic kidney and liver inflammation and fibrosis. PLOS ONE 2015;**10**:e0119662.

43 Nikolic-Paterson DJ, Wang S, Lan HY. Macrophages promote renal fibrosis through direct and indirect mechanisms. Kidney Int Suppl 2014;**4**:34–8.

44 Yan L, Mathew L, Chellan B *et al*. S100/Calgranulin-mediated inflammation accelerates left ventricular hypertrophy and aortic valve sclerosis in chronic kidney disease in a receptor for advanced glycation end products-dependent manner. Arterioscler Thromb Vasc Biol 2014;**34**:1399–411.

45 Wu Y, Li Y, Zhang C *et al*. S100a8/a9 released by CD11b+Gr1+ neutrophils activates cardiac fibroblasts to initiate angiotensin II-Induced cardiac inflammation and injury. Hypertension 2014;**63**:1241–50.

46 Leemans JC, Stokman G, Claessen N *et al*. Renal-associated TLR2 mediates ischemia/reperfusion injury in the kidney. J Clin Invest 2005;**115**:2894–903.

47 Grande MT, Sánchez-Laorden B, López-Blau C *et al*. Snail1-induced partial epithelial-to-mesenchymal transition drives renal fibrosis in mice and can be targeted to reverse established disease. Nat Med 2015;**21**:989–97.

48 Jin Q, Chen H, Luo A, Ding F, Liu Z. S100A14 stimulates cell proliferation and induces cell apoptosis at different concentrations via receptor for advanced glycation end products (RAGE). PLoS One 2011;**6**:e19375.

49 Yui S, Mikami M, Tsurumaki K, Yamazaki M. Growth-inhibitory and apoptosis-inducing activities of calprotectin derived from inflammatory exudate cells on normal fibroblasts: regulation by metal ions. J Leukoc Biol 1997;**61**:50–7.

50 Yui S, Nakatani Y, Mikami M. Calprotectin (S100A8/S100A9), an inflammatory protein complex from neutrophils with a broad apoptosis-inducing activity. Biol Pharm Bull 2003;**26**:753–60.

51 Yang L, Besschetnova TY, Brooks CR, Shah JV, Bonventre JV. Epithelial cell cycle arrest in G2/M mediates kidney fibrosis after injury. Nat Med 2010;**16**:535–43.

Supporting Information

Additional Supporting information may be found in the online version of this article at the publisher's web-site:

Table S1. Reverse transcriptase–polymerase chain reaction (RT–PCR) primer sequences

Table S2. Antibodies list Western blot

Fig. S1. Cellular expression of S100A8/A9 after 14 days of unilateral ureteral obstruction (UUO). Representative pictures of immunofluorescence staining on kidney tissue from WT mice, 14 days post-UUO, with S100A8 or S100A9 (red), DolichosBiflorus Agglutinin (DBA: collecting duct marker) and lotus tetragonolobus lectin (LTL: proximal tubule marker), both in green. Nuclei were stained with Hoechst (blue). S100A8 or S100A9, DBA and Hoechst-positive staining are merged (magnification ×40).

Fig. S2. Effect of S100A8/A9 on a polarized system of tubular epithelial cells. Representative pictures of ZO-1 and E-cadherin immunofluorescence staining of Madin–Darby canine kidney (MDCK) cell line, cultured on collagen-coated coverslip in HK2 medium and stimulated with increasing concentration of rS100A8/A9 for 24 h. Both primary antibodies were detected with an Alexa-Fluor 488 conjugated secondary antibody. Hoechst was used for nuclear staining. Magnification ×40.

Fig. S3. Effect of S100A8/A9 on epithelial cell death after ligand activation. Caspase-3 enzyme activity measurement by DEVD-AMC) cleavage. IM-TECs were stimulated for 24 h with rS100A8/A9 in the presence or not of Toll-like receptor (TLR)-4 inhibitor (CLI095) and receptor for advanced glycation end-products (RAGE) antagonist (FPSZM-1). Staurosporine (stauro) and a PAN-caspase inhibitor Q-VD-OPh hydrate (QVD) were used as experimental controls. Statistical differences were analysed by two-tailed Student's *t*-test Data are expressed as mean ± standard error of the mean (s.e.m). ***$P < 0{\cdot}0005$ *versus* unstimulated control (white bar).

